Computers and Concrete, *Vol. 21, No. 1 (2018) 31-37*
DOI: https://doi.org/10.12989/cac.2018.21.1.031

The effect of Fe_2O_3 nanoparticles instead cement on the stability of fluid-conveying concrete pipes based on exact solution

Alireza Zamani Nouri*

Department of Civil Engineering, College of Engineering, Saveh Branch, Islamic Azad University, Saveh, Iran

(Received June 17, 2017, Revised September 17, 2017, Accepted September 25, 2017)

Abstract. This paper deals with the stability analysis of concrete pipes mixed with nanoparticles conveying fluid. Instead of cement, the Fe_2O_3 nanoparticles are used in construction of the concrete pipe. The Navier-Stokes equations are used for obtaining the radial force of the fluid. Mori-Tanaka model is used for calculating the effective material properties of the concrete pipe-Fe_2O_3 nanoparticles considering the agglomeration of the nanoparticles. The first order shear deformation theory (FSDT) is used for mathematical modeling of the structure. The motion equations are derived based on energy method and Hamilton's principal. An exact solution is used for stability analysis of the structure. The effects of fluid, volume percent and agglomeration of Fe_2O_3 nanoparticles, magnetic field and geometrical parameters of pipe are shown on the stability behaviour of system. Results show that considering the agglomeration of Fe_2O_3 nanoparticles, the critical fluid velocity of the concrete pipe is decreased.

Keywords: concrete pipe; Fe_2O_3 nanoparticles; conveying fluid; stability; agglomeration

1. Introduction

The circular and reinforced concrete pipe is a highly recommended product for construction of drainage systems, storm drains, culverts and even irrigation systems. This type of pipe shows good strength and performance properties and is also cost effective compared to other drainage construction materials. There are several reasons why the concrete pipe remains the most preferred in major applications. These include design life from 70 to 100 years, cost-effective in the long run, high beam strength, lower maintenance requirements and much more affordable for very big projects.

Flexural strength of self-compacting concrete with different amount of ZnO_2 nanoparticles was investigated by Nazari and Riahi (2011). ZnO_2 nanoparticles with the average particle size of 15 nm were added partially to self-compacting concrete and flexural strength of the specimens has been measured. A new calculation method was developed by Zhu *et al*. (2013) based on these properties and an explicit iterative algorithm. The effects of two different types of SiO_2 nanoparticles (N and M series) with different ratios on the workability and compressive strength of developed binary blended concretes cured in water and lime solution as two different curing media were studied by Najigivi *et al*. (2013). Potapov *et al*. (2013) used SiO_2 nanoparticles, introducing them as stable aqueous sols from hydrothermal solutions, to enhance the mechanical properties of concrete. Effects of magnetic water on different properties of cement paste including fluidity, compressive strength, time of setting was studied by Khorshidi *et al*. (2014). A 100 mm-diameter split Hopkinson pressure bar (SHPB) was applied by Li *et al* (2016) to investigate effects of nanoparticles on the dynamic mechanical properties of recycled aggregate concrete (RAC) under impact loading. Ismael *et al*. (2016) developed aiming at analyzing the influence on the latter, and as a consequence on cracking, of nano-Al_2O_3 and nano-SiO_2 additions. The nano-SiO_2 (NS) and nano-$CaCO_3$ (NC) were incorporated to replace cement by mass of 1 and 2% in RACs. Palla *et al*. (2017) studied the effect of silica nanoparticles (SNPs) in high volume fly ash (40% replacement) cement paste, mortar and concrete. The content of SNPs (0.5-3.0%) was added by the weight of binder and w/b ratio (0.23, 0.25 & 3.0) was optimized in paste and mortar system. Recently, vibration and stability of concrete pipes reinforced with carbon nanotubes (CNTs) conveying fluid were presented by Zamani Nouri (2017). Due to the existence of CNTs, the structure was subjected to magnetic field.

In this paper, the stability analysis of concrete pipes conveying fluid is presented for the first time. The concrete pipe is reinforced by Fe_2O_3 nanoparticles where the Mori-Tanaka model is used for modeling and considering agglomeration effects. Based on FSDT, energy method and Hamilton's principle, the motion equations are derived and solved by an exact solution. The effects of the fluid, volume percent and agglomeration of Fe_2O_3 nanoparticles, magnetic field and geometrical parameters on the stability analysis of the structure are investigated.

2. Mathematical modeling

A fluid-conveying concrete pipe reinforced with Fe_2O_3

*Corresponding author, Ph.D.
E-mail: Dr.zamani.ar@gmail.com

ISSN: 1598-8198 (Print), 1598-818X (Online)

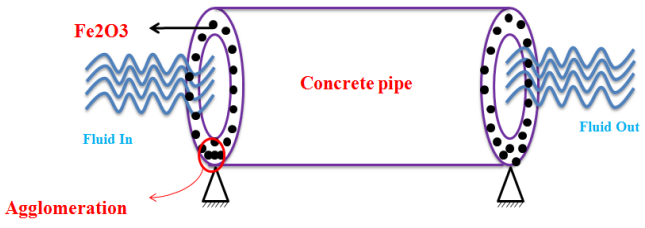

Fig. 1 A fluid-conveying concrete pipe reinforced with Fe_2O_3 nanoparticles

nanoparticles is shown in Fig. 1 where the agglomeration effect of Fe_2O_3 nanoparticles is considered.

2.1 FSDT

Based on FSDT shell theory, the displacement field can be expressed as (Brush and Almroth 1975)

$$u(x,\theta,z,t)=u(x,\theta,t)+z\phi_x(x,\theta,t), \tag{1a}$$

$$v(x,\theta,z,t)=v(x,\theta,t)+z\phi_\theta(x,\theta,t), \tag{1b}$$

$$w(x,\theta,z,t)=w(x,\theta,t), \tag{1c}$$

where ($u(x,\theta,z,t)$, $v(x,\theta,z,t)$, $w(x,\theta,z,t)$) denote the displacement components at an arbitrary point (x,θ,z) in the shell, and ($u(x,\theta,t)$, $v(x,\theta,t)$, $w(x,\theta,t)$) are the displacement of a material point at (x,θ) on the mid-plane (i.e., z=0) of the shell along the x-, θ-, and z-directions, respectively; ϕ_x and ϕ_θ are the rotations of the normal to the mid-plane about x- and θ- directions, respectively. Based on above relations, the strain-displacement equations may be written as

$$\varepsilon_{xx}=\frac{\partial u}{\partial x}+z\frac{\partial \phi_x}{\partial x}, \tag{2a}$$

$$\varepsilon_{\theta\theta}=\frac{1}{R}\left(w+\frac{\partial v}{\partial \theta}\right)+\frac{z}{R}\frac{\partial \phi_\theta}{\partial \theta}, \tag{2b}$$

$$\gamma_{x\theta}=\frac{\partial v}{\partial x}+\frac{1}{R}\left(\frac{\partial u}{\partial \theta}\right)+z\left(\frac{\partial \phi_\theta}{\partial x}+\frac{1}{R}\frac{\partial \phi_x}{\partial \theta}\right), \tag{2c}$$

$$\gamma_{xz}=\phi_x+\frac{\partial w}{\partial x}, \tag{2d}$$

$$\gamma_{z\theta}=\frac{1}{R}\left(\frac{\partial w}{\partial \theta}-v\right)+\phi_\theta, \tag{2e}$$

where (ε_{xx}, $\varepsilon_{\theta\theta}$) are the normal strain components and ($\gamma_{\theta z}$, γ_{xz}, $\gamma_{x\theta}$) are the shear strain components.

2.2 Energy method

The potential energy can be written as

$$U=\frac{1}{2}\int\left(\sigma_{xx}\varepsilon_{xx}+\sigma_{yy}\varepsilon_{yy}+\tau_{xz}\gamma_{xz}+\tau_{yz}\gamma_{yz}+\tau_{xy}\gamma_{xy}\right)dV. \tag{3}$$

Combining of Eqs. (1)-(3) yields

$$\begin{aligned}U=\frac{1}{2}\int_0^{2\pi}\int_0^L\Bigg\{&\left[N_{xx}\frac{\partial u}{\partial x}+M_{xx}\frac{\partial \phi_x}{\partial x}\right]+\left[N_{yy}\frac{\partial v}{\partial y}+M_{yy}\frac{\partial \phi_y}{\partial y}\right]\\&+Q_x\left(\phi_x+\frac{\partial w}{\partial x}\right)+N_{xy}\left[\frac{\partial v}{\partial x}+\frac{\partial u}{\partial y}\right]\\&+M_{xy}\left[\frac{\partial \phi_y}{\partial x}+\frac{\partial \phi_x}{\partial y}\right]+Q_y\left[\frac{\partial w}{\partial y}+\phi_y\right]\Bigg\}dA,\end{aligned} \tag{4}$$

where the stress resultant-displacement relations can be written as

$$\begin{Bmatrix}N_{xx}\\N_{yy}\\N_{xy}\end{Bmatrix}=\int_{-\frac{h}{2}}^{\frac{h}{2}}\begin{Bmatrix}\sigma_{xx}^c\\\sigma_{yy}^c\\\tau_{xy}^c\end{Bmatrix}dz, \tag{5}$$

$$\begin{Bmatrix}Q_x\\Q_\theta\end{Bmatrix}=k'\int_{-\frac{h}{2}}^{\frac{h}{2}}\begin{Bmatrix}\tau_{xz}^c\\\tau_{yz}^c\end{Bmatrix}dz, \tag{6}$$

$$\begin{Bmatrix}M_{xx}\\M_{yy}\\M_{xy}\end{Bmatrix}=\int_{-\frac{h}{2}}^{\frac{h}{2}}\begin{Bmatrix}\sigma_{xx}^c\\\sigma_{yy}^c\\\tau_{xy}^c\end{Bmatrix}z\,dz. \tag{7}$$

In which k' is shear correction coefficient. The kinetic energy of system may be written as

$$K=\frac{\rho}{2}\int\left(\left(\frac{\partial u}{\partial t}+z\frac{\partial \phi_x}{\partial t}\right)^2+\left(\frac{\partial v}{\partial t}+z\frac{\partial \phi_y}{\partial t}\right)^2+\left(\frac{\partial w}{\partial t}\right)^2\right)dV. \tag{8}$$

Defining the moments of inertia as below

$$\begin{Bmatrix}I_0\\I_1\\I_2\end{Bmatrix}=\int_{-h/2}^{h/2}\begin{bmatrix}\rho\\\rho z\\\rho z^2\end{bmatrix}dz, \tag{9}$$

the kinetic energy may be written as

$$\begin{aligned}K=\frac{1}{2}\int&\left(I_0\left(\left(\frac{\partial u}{\partial t}\right)^2+\left(\frac{\partial v}{\partial t}\right)^2+\left(\frac{\partial w}{\partial t}\right)^2\right)+I_1\left(2\frac{\partial u}{\partial t}\frac{\partial \phi_x}{\partial t}+2\frac{\partial v}{\partial t}\frac{\partial \phi_y}{\partial t}\right)\right.\\&\left.+I_2\left(\left(\frac{\partial \phi_x}{\partial t}\right)^2+\left(\frac{\partial \phi_y}{\partial t}\right)^2\right)\right)dA.\end{aligned} \tag{10}$$

The work done by the magnetic field can be written as (Agrawal *et al.* 2016)

$$W_m=\int_{-h/2}^{h/2}\underbrace{\eta h H_x^2\left(\frac{\partial^2 w}{\partial x^2}\right)}_{F_{magnet}}dz, \tag{11}$$

where η and H_x are magnetic permeability and magnetic field, respectively.

The governing equation of the fluid can be described by the well-known Navier-Stokes equation as below (Baohui *et al.* 2012)

$$\rho_f\frac{d\mathbf{V}}{dt}=-\nabla\mathbf{P}+\mu\nabla^2\mathbf{V}+\mathbf{F}_{body}, \tag{12}$$

where $V\equiv(v_z, v_\theta, v_x)$ is the flow velocity vector in cylindrical coordinate system with components in longitudinal x, circumferential θ and radial z directions. Also, P, μ and ρ_f are the pressure, the viscosity and the density of the fluid, respectively and F_{body} denotes the body forces. In Navier-Stokes equation, the total derivative operator with respect to $t$is

$$\frac{d}{dt}=\frac{\partial}{\partial t}+v_x\frac{\partial}{\partial x}+v_\theta\frac{\partial}{R\partial\theta}+v_z\frac{\partial}{\partial z}. \tag{13}$$

At the point of contact between the fluid and the core, the relative velocity and acceleration in the radial direction are equal. So

$$v_z=\frac{dw}{dt}. \tag{14}$$

By employing Eqs. (13) and (14) and substituting into Eq. (12), the pressure inside the pipe can be computed as

$$\frac{\partial p_z}{\partial z}=-\rho_f\left(\frac{\partial^2 w}{\partial t^2}+2v_x\frac{\partial^2 w}{\partial x\,\partial t}+v_x{}^2\frac{\partial^2 w}{\partial x^2}\right)+\mu\left(\frac{\partial^3 w}{\partial x^2\,\partial t}+\frac{\partial^3 w}{R^2\partial\theta^2\,\partial t}+v_x\left(\frac{\partial^3 w}{\partial x^3}+\frac{\partial^3 w}{R^2\partial\theta^2\,\partial x}\right)\right). \tag{15}$$

By multiplying two sides of Eq. (16) in the inside area of the pipe (A), the radial force in the pipe is calculated as below

$$F_{fluid}=A\frac{\partial p_z}{\partial z}=-\rho_f\left(\frac{\partial^2 w}{\partial t^2}+2v_x\frac{\partial^2 w}{\partial x\,\partial t}+v_x{}^2\frac{\partial^2 w}{\partial x^2}\right)+\mu\left(\frac{\partial^3 w}{\partial x^2\,\partial t}+\frac{\partial^3 w}{R^2\partial\theta^2\,\partial t}+v_x\left(\frac{\partial^3 w}{\partial x^3}+\frac{\partial^3 w}{R^2\partial\theta^2\,\partial x}\right)\right). \tag{16a}$$

Finally, the external work due to the pressure of the fluid may be obtained as follows

$$W_f=\int(F_{fluid})w\,dA=\int\left(-\rho_f\left(\frac{\partial^2 w}{\partial t^2}+2v_x\frac{\partial^2 w}{\partial x\,\partial t}+v_x{}^2\frac{\partial^2 w}{\partial x^2}\right)+\mu\left(\frac{\partial^3 w}{\partial x^2\,\partial t}+\frac{\partial^3 w}{R^2\partial\theta^2\,\partial t}+v_x\left(\frac{\partial^3 w}{\partial x^3}+\frac{\partial^3 w}{R^2\partial\theta^2\,\partial x}\right)\right)\right)w\,dA. \tag{16b}$$

Finally, applying Hamilton's principal, the motion equations can be derived as

$$\delta u:\frac{\partial N_{xx}}{\partial x}+\frac{\partial N_{xy}}{\partial y}=I_0\frac{\partial^2 u}{\partial t^2}+I_1\frac{\partial^2\phi_x}{\partial t^2}, \tag{17}$$

$$\delta v:\frac{\partial N_{xy}}{\partial x}+\frac{\partial N_{yy}}{\partial y}=I_0\frac{\partial^2 v}{\partial t^2}+I_1\frac{\partial^2\phi_y}{\partial t^2}, \tag{18}$$

$$\delta w:\frac{\partial Q_x}{\partial x}+\frac{\partial Q_y}{\partial y}+\eta hH_x^2\left(\frac{\partial^2 w}{\partial x^2}\right)-\rho_f\left(\frac{\partial^2 w}{\partial t^2}+2v_x\frac{\partial^2 w}{\partial x\,\partial t}+v_x{}^2\frac{\partial^2 w}{\partial x^2}\right)+\mu\left(\frac{\partial^3 w}{\partial x^2\,\partial t}+\frac{\partial^3 w}{R^2\partial\theta^2\,\partial t}+v_x\left(\frac{\partial^3 w}{\partial x^3}+\frac{\partial^3 w}{R^2\partial\theta^2\,\partial x}\right)\right)=I_0\frac{\partial^2 w}{\partial t^2}, \tag{19}$$

$$\delta\phi_x:\frac{\partial M_{xx}}{\partial x}+\frac{\partial M_{xy}}{\partial y}-Q_x=I_2\frac{\partial^2\phi_x}{\partial t^2}+I_1\frac{\partial^2 u}{\partial t^2}, \tag{20}$$

$$\delta\varphi_y:\frac{\partial M_{xy}}{\partial x}+\frac{\partial M_{xx}}{\partial y}-Q_y=I_2\frac{\partial^2\phi_y}{\partial t^2}+I_1\frac{\partial^2 v}{\partial t^2}. \tag{21}$$

2.3 Mori-Tanaka model

Using Mori-Tanaka model, the matrix is assumed to be isotropic and elastic, with the Young's modulus E_m and the Poisson's ratio υ_m. The experimental results show that the assumption of uniform dispersion for nanoparticles in the matrix is not correct and the most of nanoparticles are bent and centralized in one area of the matrix. These regions with concentrated nanoparticles are assumed to have spherical shapes, and are considered as ''inclusions'' with different elastic properties from the surrounding material. The total volume V_r of nanoparticles can be divided into the following two parts (Shi and Feng 2004)

$$V_r=V_r^{inclusion}+V_r^{m}, \tag{22}$$

where $V_r^{inclusion}$ and V_r^{m} are the volumes of nanoparticles dispersed in the spherical inclusions and in the matrix, respectively. Introduce two parameters ξ and ζ describe the agglomeration of nanoparticles

$$\xi=\frac{V_{inclusion}}{V}, \tag{23}$$

$$\zeta=\frac{V_r^{inclusion}}{V_r}. \tag{24}$$

However, the average volume fraction c_r of nanoparticles in the composite is

$$C_r=\frac{V_r}{V}. \tag{25}$$

Assume that all the orientations of the nanoparticles are completely random. Hence, the effective bulk modulus (K) and effective shear modulus (G) may be written as

$$K=K_{out}\left[1+\frac{\xi\left(\frac{K_{in}}{K_{out}}-1\right)}{1+\alpha(1-\xi)\left(\frac{K_{in}}{K_{out}}-1\right)}\right], \tag{26}$$

$$G=G_{out}\left[1+\frac{\xi\left(\frac{G_{in}}{G_{out}}-1\right)}{1+\beta(1-\xi)\left(\frac{G_{in}}{G_{out}}-1\right)}\right], \tag{27}$$

where

$$K_{in}=K_m+\frac{(\delta_r-3K_m\chi_r)C_r\zeta}{3(\xi-C_r\zeta+C_r\zeta\chi_r)}, \tag{28}$$

$$K_{out}=K_m+\frac{C_r(\delta_r-3K_m\chi_r)(1-\zeta)}{3\left[1-\xi-C_r(1-\zeta)+C_r\chi_r(1-\zeta)\right]}, \tag{29}$$

$$G_{in} = G_m + \frac{(\eta_r - 3G_m\beta_r)C_r\zeta}{2(\xi - C_r\zeta + C_r\zeta\beta_r)}, \tag{30}$$

$$G_{out} = G_m + \frac{C_r(\eta_r - 3G_m\beta_r)(1-\zeta)}{2\left[1-\xi - C_r(1-\zeta) + C_r\beta_r(1-\zeta)\right]}, \tag{31}$$

where χ_r, β_r, δ_r, η_r may be calculated as

$$\chi_r = \frac{3(K_m + G_m) + k_r - l_r}{3(k_r + G_m)}, \tag{32}$$

$$\beta_r = \frac{1}{5}\left\{\frac{4G_m + 2k_r + l_r}{3(k_r + G_m)} + \frac{4G_m}{(p_r + G_m)} + \frac{2\left[G_m(3K_m + G_m) + G_m(3K_m + 7G_m)\right]}{G_m(3K_m + G_m) + m_r(3K_m + 7G_m)}\right\}, \tag{33}$$

$$\delta_r = \frac{1}{3}\left[n_r + 2l_r + \frac{(2k_r - l_r)(3K_m + 2G_m - l_r)}{k_r + G_m}\right], \tag{34}$$

$$\eta_r = \frac{1}{5}\left[\frac{2}{3}(n_r - l_r) + \frac{4G_m p_r}{(p_r + G_m)} + \frac{8G_m m_r(3K_m + 4G_m)}{3K_m(m_r + G_m) + G_m(7m_r + G_m)} + \frac{2(k_r - l_r)(2G_m + l_r)}{3(k_r + G_m)}\right], \tag{35}$$

where k_r, l_r, n_r, p_r, m_r are the Hills elastic modulus; K_m and G_m are the bulk and shear moduli of the matrix which can be written as

$$K_m = \frac{E_m}{3(1-2\upsilon_m)}, \tag{36}$$

$$G_m = \frac{E_m}{2(1+\upsilon_m)}. \tag{37}$$

Furthermore, β, α can be obtained from

$$\alpha = \frac{(1+\upsilon_{out})}{3(1-\upsilon_{out})}, \tag{38}$$

$$\beta = \frac{2(4-5\upsilon_{out})}{15(1-\upsilon_{out})}, \tag{39}$$

$$\upsilon_{out} = \frac{3K_{out} - 2G_{out}}{6K_{out} + 2G_{out}}. \tag{40}$$

Finally, the elastic modulus (E) and poison's ratio (υ) can be calculated as

$$E = \frac{9KG}{3K + G}, \tag{41}$$

$$\upsilon = \frac{3K - 2G}{6K + 2G}. \tag{42}$$

2.4 Final motion equations

Substituting stress-strain relations from Hook's law into Eqs. (5)-(7), the stress resultant-displacement relations can be obtained as follow

$$N_{xx} = A_{110}\frac{\partial u}{\partial x} + A_{111}\frac{\partial \phi_x}{\partial x} + A_{120}\frac{\partial v}{\partial y} + A_{121}\frac{\partial \phi_y}{\partial y}, \tag{43}$$

$$N_{yy} = A_{120}\frac{\partial u}{\partial x} + A_{121}\frac{\partial \phi_x}{\partial x} + A_{220}\frac{\partial v}{\partial y} + A_{221}\frac{\partial \phi_y}{\partial y}, \tag{44}$$

$$Q_y = k' A_{44}\left[\frac{\partial w}{\partial y} + \phi_y\right], \tag{45}$$

$$Q_x = k' A_{55}\left(\frac{\partial w}{\partial x} + \phi_x\right), \tag{46}$$

$$N_{xy} = A_{660}\left(\frac{\partial u}{\partial y} + \frac{\partial v}{\partial x}\right) + A_{661}\left(\frac{\partial \phi_x}{\partial y} + \frac{\partial \phi_y}{\partial x}\right), \tag{47}$$

$$M_{xx} = A_{111}\frac{\partial u}{\partial x} + A_{112}\frac{\partial \phi_x}{\partial x} + A_{121}\frac{\partial v}{\partial y} + A_{122}\frac{\partial \phi_y}{\partial y}, \tag{48}$$

$$M_{yy} = A_{121}\frac{\partial u}{\partial x} + A_{122}\frac{\partial \phi_x}{\partial x} + A_{221}\frac{\partial v}{\partial y} + A_{222}\frac{\partial \phi_y}{\partial y}, \tag{49}$$

$$M_{xy} = A_{661}\left(\frac{\partial u}{\partial y} + \frac{\partial v}{\partial x}\right) + A_{662}\left(\frac{\partial \phi_x}{\partial y} + \frac{\partial \phi_\theta}{\partial x}\right), \tag{50}$$

where

$$A_{11k} = \int_{-h/2}^{h/2} Q_{11} z^k dz, \qquad k = 0,1,2 \tag{51}$$

$$A_{12k} = \int_{-h/2}^{h/2} Q_{12} z^k dz \qquad k = 0,1,2 \tag{52}$$

$$A_{22k} = \int_{-h/2}^{h/2} Q_{22} z^k dz, \qquad k = 0,1,2 \tag{53}$$

$$A_{66k} = \int_{-h/2}^{h/2} Q_{66} z^k dz, \qquad k = 0,1,2 \tag{54}$$

$$A_{44} = \int_{-h/2}^{h/2} Q_{44} dz, \tag{55}$$

$$A_{55} = \int_{-h/2}^{h/2} Q_{55} dz. \tag{56}$$

Substituting Eqs. (43)-(50) into Eqs. (17)-(21) yields the motion equations in terms of displacement.

3. Solution

Steady state solutions to the governing equations of the system motion and the electric potential distribution which relate to the simply supported boundary conditions and zero electric potential along the edges of the surface electrodes can be assumed as

$$u(x, y, t) = u_0 \cos\left(\frac{n\pi x}{L}\right)\sin\left(\frac{m\pi y}{b}\right)e^{i\omega t}, \tag{57}$$

Table 1 Validation of present work

n	Qu *et al*. (2013)	Tang *et al*. (2016)	Present
1	0.016103	0.016101	0.016234
2	0.009382	0.011225	0.011714
3	0.022105	0.022310	0.024903
4	0.042095	0.042139	0.044935
5	0.068008	0.068024	0.070857
6	0.099730	0.099738	0.102591
7	0.137239	0.137240	0.140108
8	0.180528	0.180530	0.183402
9	0.229594	0.229596	0.232472
10	0.284436	0.284439	0.287318

$$v(x,y,t)=v_0\sin(\frac{n\pi x}{L})\cos(\frac{m\pi y}{b})e^{i\omega t}, \quad (58)$$

$$w(x,y,t)=w_0\sin(\frac{n\pi x}{L})\sin(\frac{m\pi y}{b})e^{i\omega t}, \quad (59)$$

$$\phi_x(x,y,t)=\psi_{x0}\cos(\frac{n\pi x}{L})\sin(\frac{m\pi y}{b})e^{i\omega t}, \quad (60)$$

$$\phi_y(x,y,t)=\psi_{y0}\sin(\frac{n\pi x}{L})\cos(\frac{m\pi y}{b})e^{i\omega t}. \quad (61)$$

Substituting Eqs. (57)-(61) into motion equations yields

$$\begin{bmatrix} K_{11} & K_{12} & K_{13} & K_{14} & K_{15} & K_{16} \\ K_{21} & K_{22} & K_{23} & K_{24} & K_{25} & K_{26} \\ K_{31} & K_{32} & K_{33} & K_{34} & K_{35} & K_{36} \\ K_{41} & K_{42} & K_{43} & K_{44} & K_{45} & K_{46} \\ K_{51} & K_{52} & K_{53} & K_{54} & K_{55} & K_{56} \\ K_{61} & K_{62} & K_{63} & K_{64} & K_{65} & K_{66} \end{bmatrix} \begin{bmatrix} u_0 \\ v_0 \\ w_0 \\ \psi_{x0} \\ \psi_{y0} \\ \varphi_0 \end{bmatrix} = 0, \quad (62)$$

where K_{ij} are constants. Finally, for calculating the frequency of the system (ω), the determinant of matrix in Eq. (62) should be equal to zero.

4. Result and dissection

A computer program is prepared for the stability solution of concrete pipe reinforced with Fe_2O_3 nanoparticles. The Fe_2O_3 nanoparticles have Yong's modulus of E_r=160 GPa and Poisson's ratio of ν_r=0.3. In addition, the concrete pipe have Yong's modulus of E_m=20 GPa and Poisson's ratio of ν_m=0.3.

To the best author's knowledge, no similar publications for vibration and instability of FG-CNTRC pipes cannot found directly. However, the present work could be partially validated based on a simplified analysis suggested by Qu *et al*. (2013), Tang *et al*. (2016). However, vibration of simply supported classical cylindrical shells is investigated where the nonlinear terms in motion equations, fluid, elastomeric foundation, thermal gradient and SWCNTs as reinforcer are ignored. The structure parameters of the classical shell assumed as h/R=0.01, L/R=20, E=210 GPa, ν=0.3, ρ=7850 Kg/m^3. A non-dimensional frequency is defined as. Table 3 illustrates the frequency of pipe for classical theory. As can be seen, the obtained results are close to those expressed in Qu *et al*. (2013), Tang *et al*. (2016), indicating validation of our work. It should be noted that a little difference between the results of other works and present work is due to the fact that in this study, Donnel classical shell theory is considered for validation while in other mentioned works, the Sanders classical shell theory is applied.

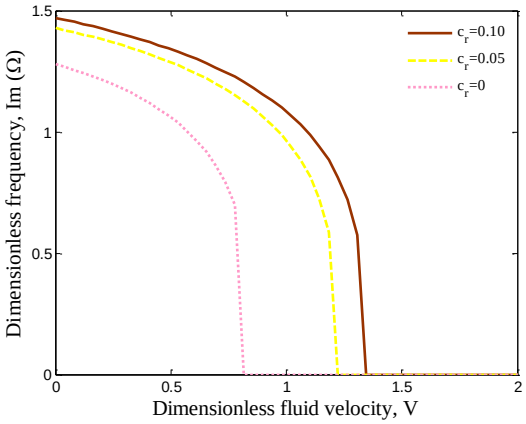

Fig. 2 The effect of Fe_2O_3 nanoparticles volume percent on the frequency of structure

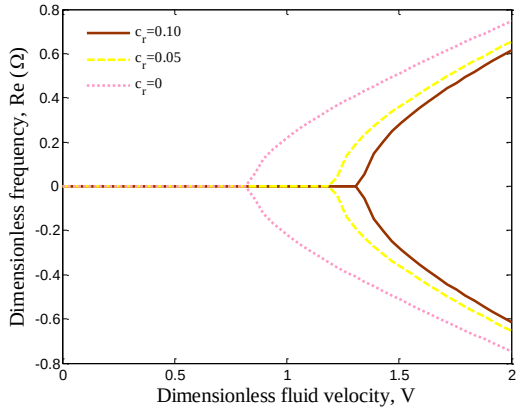

Fig. 3 The effect of Fe_2O_3 nanoparticles volume percent on the damping of structure

Figs. 2 and 3 show the Fe_2O_3 nanoparticles volume percent on the frequency (Im(Ω)) and damping (Re(Ω)) of structure ($\Omega=\sqrt{C_{11}/\rho_f}\,\omega$) versus flow velocity ($V=\sqrt{\rho_f/C_{11}}\,v_x$,) in the dimensionless form, respectively. As can be seen, Im(Ω) decreases with increasing V, while the Re(Ω) remains zero. These imply that the system is stable. When the natural frequency becomes zero, critical velocity is reached, which the system loses its stability due to the divergence via a pitchfork bifurcation. Hence, the Eigen frequencies have the positive real parts, which the system becomes unstable. In this state, both real and imaginary parts of frequency become zero at the same point. Therefore, with increasing flow velocity, system stability decreases and became susceptible to buckling. Furthermore, increasing Fe_2O_3 nanoparticles yields to increases in the Im(Ω). This is because increasing the Fe_2O_3 nanoparticles volume percent implies stiffer structure.

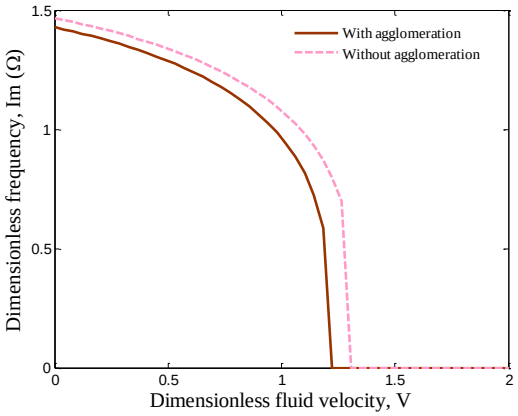

Fig. 4 The effect of Fe_2O_3 nanoparticles agglomeration on the frequency of structure

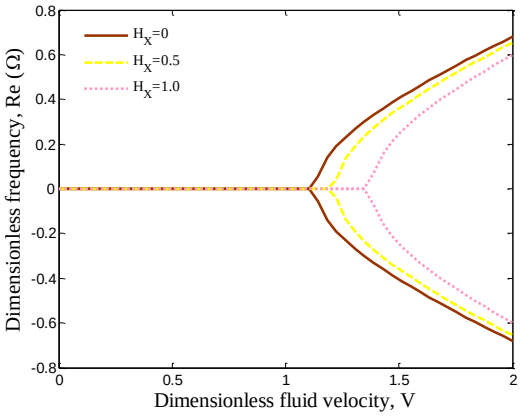

Fig. 7 The effect of magnetic field on the damping of structure

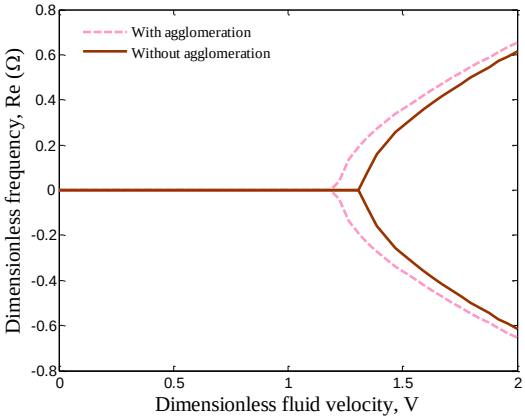

Fig. 5 The effect of Fe_2O_3 nanoparticles agglomeration on the damping of structure

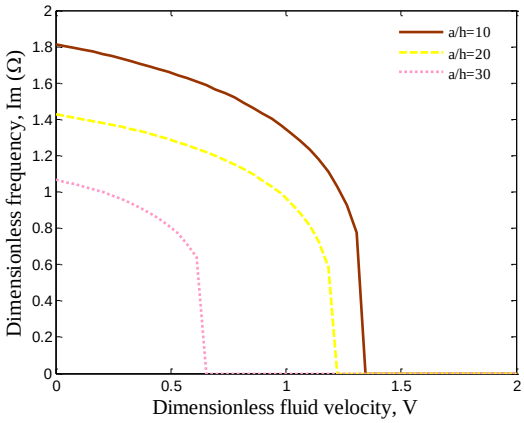

Fig. 8 The effect of length to thickness ratio on the frequency of structure

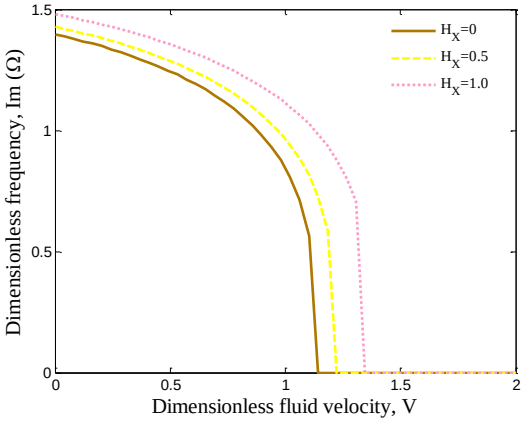

Fig. 6 The effect of magnetic field on the frequency of structure

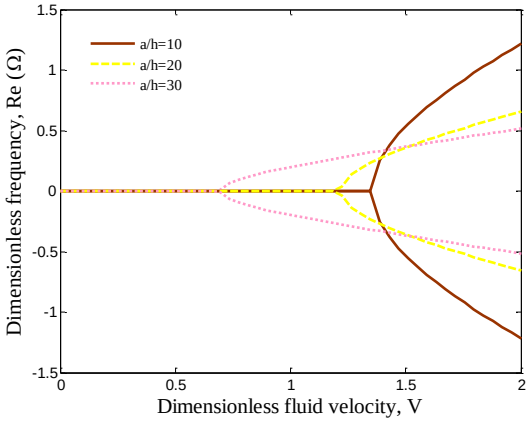

Fig. 9 The effect of length to thickness ratio on the damping of structure

The agglomeration effects of Fe_2O_3 nanoparticles are shown in Figs. 4 and 5 on the dimensionless frequency and damping of concrete pipe. It can be seen that considering agglomeration effects, the frequency and critical fluid velocity are decreased. It is because with considering agglomeration effects, the stability of the structure decreases.

In realizing the influence of magnetic field, Figs. 6 and 7 show how dimensionless frequency and damping of concrete pipe changes with respect to dimensionless fluid velocity. It is found that from Fig. 4, the Im(Ω) and critical flow velocity for the structure increase with the increase of magnetic field. It is due to the fact that with increasing the magnetic field, the stiffness of structure increases.

Figs. 8 and 9 illustrate the effect of length to thickness ratio (a/h) on the Im(Ω) and Re(Ω) versus V, respectively. The results indicate that with increasing length to thickness ratio, the frequency and critical flow velocity of concrete

pipe are decreased. It is because with increasing length to thickness ratio, the stiffness of structure is decreased.

5. Conclusions

Stability analysis of a concrete pipe conveying fluid was studied in this work. Instead % of cement, the Fe_2O_3 nanoparticles was used. The Mori-Tanaka model was applied for calculating the effective material properties of the structure considering agglomeration effects. Based on FSDT, energy method and Hamilton's principle, the motion equations were derived. Based on an exact solution, the frequency and critical fluid velocity of the structure were obtained. The effects of different parameters such as Fe_2O_3 nanoparticles volume percent and agglomeration, magnetic field and length to thickness ration of the pipe were shown on the frequency and critical fluid velocity of the structure. The important findings of this work were:

√ Increasing volume percent of Fe_2O_3 nanoparticles, increased frequency and critical fluid velocity.

√ Considering agglomeration effects, the frequency and critical fluid velocity were decreased.

√ With increasing flow velocity, system stability decreases and became susceptible to buckling.

√ Applying the magnetic field to the structure leads to higher frequency and critical fluid velocity.

√ With increasing length to thickness ratio, the frequency and critical fluid velocity of structure were decreased.

Reference

Agrawal, S., Gupta, V.K. and Kankar, P.K. (2016), "Static analysis of magnetic field affected double single walled carbon nanotube system", *Proced. Tech.*, **23**, 84-90.

Baohui, L., Hangshan, G., Yongshou, L. nd Zhufeng, Y. (2012), "Free vibration analysis of micropipe conveying fluid by wave method", *Resul. Phys.*, **2**, 104-109.

Brush, D.O. and Almroth, B.O. (1975), *Buckling of Bars, Plates and Shells*, McGraw-Hill, New York.

Ismael, R., Silva, J.V., Carmo, R.N.F., Soldado, E. and Júlio, E. (2016), "Influence of nano-SiO_2 and nano-Al2O3 additions on steel-to-concrete bonding", *Constr. Build. Mater.*, **125**, 1080-1092.

Khorshidi, N., Ansari, M. and Bayat, M. (2014), "An investigation of water magnetization and its influence on some concrete specificities like fluidity and compressive strength", *Comput. Concrete*, **13**, 649-657.

Li, W., Luo, Zh., Long, Ch., Wu, Ch. and Shah, S.P. (2016), "Effects of nanoparticle on the dynamic behaviors of recycled aggregate concrete under impact loading", *Mater. Des.*, **112**, 58-66.

Najigivi, A., Khaloo, A., Iraji zad, A. and Abdul Rashid, S. (2013), "Investigating the effects of using different types of SiO_2 nanoparticles on the mechanical properties of binary blended concrete", *Compos. Part B: Eng.*, **54**, 52-58.

Nazari, A. and Riahi, Sh. (2011), "The effects of zinc dioxide nanoparticles on flexural strength of self-compacting concrete", *Compos. Part B: Eng.*, **42**, 167-175.

Niewiadomski, P., Ćwirzeń, A. and Hoła, J. (2015), "The influence of an additive in the form of selected nanoparticles on the physical and mechanical characteristics of self-compacting concrete", *Proced. Eng.*, **111**, 601-606.

Palla, R., Karade, S.R., Mishra, G., Sharma, U. and Singh, L.P. (2017), "High strength sustainable concrete using silica nanoparticles", *Constr. Build. Mater*., **138**, 285-295.

Potapov, V.V., Tumanov, A.V., Zakurazhnov, M.S., Cerdan, A.A., Kashutin, A.N. and Shalaev, K.S. (2013), "Enhancement of concrete durability by introducing SiO_2 nanoparticles", *Glass Phys. Chem.*, **39**, 425-430.

Qu, Y., Chen, Y., Long, X., Hua, H. and Meng, G. (2013), "Free and forced vibration analysis of uniform and stepped circular cylindrical shells using a domain decomposition method", *Appl. Acoust.*, **74**, 425-439.

Shi, D.L. and Feng, X.Q. (2004), "The effect of nanotube waviness and agglomeration on the lastic property of carbon nanotube-reinforced composties", *J. Eng. Mater. Tech.*, ASME, **126**, 250-270.

Tang, D., Wu, G., Yao, X. and Wang, Ch. (2016), "Free vibration analysis of circular cylindrical shells with arbitrary boundary conditions by the method of reverberation-ray matrix", *Shock Vib*., **3814693**, 18.

Zamani Nouri, A. (2017), "Mathematical modeling of concrete pipes reinforced with CNTs conveying fluid for vibration and stability analyses", *Comput. Concrete*, **19**(3), 325-331.

Zhu, Zh., Qiang, Sh. and Chen, W. (2013), "A new method solving the temperature field of concrete around cooling pipes", *Comput. Concrete*, **11**, 441-462.

CC